A Quantitative Study of Nanoparticle Release from Nanocoatings Exposed to UV Radiation

Lipiin Sung, Deborah Stanley, Justin M. Gorham, Savelas Rabb, Xiaohong Gu, Lee L. Yu, and Tinh Nguyen

National Institute of Standards and Technology
100 Bureau Dr, Gaithersburg, MD 20899, USA

Abstract

Nanoparticles are increasingly used in polymer coatings (i.e., nanocoatings) to improve multiple properties including the mechanical, electrical, gas barrier, and ultraviolet (UV) resistance of traditional coatings. These high performance nanocoatings are often used in outdoor environments. However, because polymers are susceptible to degradation by weathering elements, nanoparticles in a nanocoating may be released into the environments during its life cycle, which potentially poses an environmental health and safety concern and may hinder application of these advanced coatings. This study presents protocols and experimental technique to quantify the release of nanosilica from epoxy nanocoating as a function of UV exposure. Specimens of an epoxy coating containing 5 % untreated nanosilica in specially-designed holders were exposed to UV radiation (295 nm to 400 nm) in a well-controlled high-intensity UV chamber. Exposed specimens were removed at specified UV dose intervals for measurements of coating chemical degradation, mass loss, nanosilica accumulation on specimen surface, and nanosilica release as a function of UV dose. Measurement of nanosilica release was accomplished by a) periodically spraying UV-exposed specimens with water, b) collecting runoff water/released particles, and c) analyzing collected solutions by inductively coupled plasma-optical emission spectrometry (ICP-OES) using a National Institute of Standards and Technology(NIST)-developed protocol. Results demonstrated that the amount of nanosilica release was substantial and increased rapidly with UV dose. Mass loss, chemical degradation, and silica accumulation on specimen surface also increased with UV dose.

Introduction

Extensive research in the last decade has shown that polymer matrices containing particles having at least one dimension less than 100 nm (i.e., polymer nanocomposites) possess exceptional properties (1-4). These advanced composites are excellent materials for polymer coatings (nanocoatings). While applications vary widely, polymer nanocoatings generally take advantage of exceptional mechanical, gas barrier, flame retardance, self-cleaning, and ultraviolet (UV) resistance properties of nanoparticles. Polymer nanocoatings have gained strong commercial footing in the past few years, due to both their outstanding performance and the efforts of coating manufacturers who offer user-friendly products with minimum changes in the cost and manufacturing processes (5). The coating nanotechnology segment alone is projected to increase from $3.4 billion in 2010 to nearly $18 billion in 2015, an average increase of 39.5 % (6), while the nano adhesive market is projected to increase at 36.4 %, from $257 million in 2010 to $1.2 billion in 2015 (6).

Because of their exceptional properties, polymer nanocoatings are, or will potentially be, used in a variety of outdoor applications such as on automobiles, building structures, bridges, and airplanes. Whatever the application, the release of the nanoparticles from the matrix during the product's life cycle plays a key role in the commercialization and uses of these nanocomposite products. This is because nanoparticles have been shown to pose potential risks to human health and environment (7-12). There are various possible mechanisms by which nanoparticles could be released during a nano-containing product's life cycle (i.e., manufacturing, use, disposal, recycling, and incineration), including mechanical forces, matrix degradation, chemical dissolution, and incineration (12-15). As such, it is assumed that some fraction of nanoparticles that have been incorporated in the polymer matrix will be released into the environment during a product's life cycle. (Here, release is defined as the separation of polymer-free and polymer-containing particles that contain nanoparticles from the polymer nanocomposites.) Because of their potential risks to workers, particles released in the air by mechanical forces (e.g., abrasion, polishing, sanding, sawing, and drilling) from polymer nanocomposite materials (plastics and coatings) have received the most attention in the past few years (15-22). The prevailing conclusion from these studies is that the particles released from

advanced composite materials by mechanical forces remain embedded in the matrix and the size and the size distribution of the aerosolized particles are strongly dependent on the matrix.

The release of nanoparticles from polymer nanocoatings by matrix degradation is an important mechanism, because most common polymers tend to undergo some form of degradation when they are exposed to UV, moisture, temperature, or combinations thereof (23). A serious consequence of the host matrix degradation is that the embedded nanoparticles could be released to the environment via the effects of rain, condensed water, wind, and mechanical vibrations. Several studies on the fate of nanoparticles in polymer nanocomposites and their coatings during exposure to a weathering environment have been reported (24-27). By means of microscopy, these studies showed that a substantial amount of embedded nanoparticles were accumulating on the nanocomposite surface during exposures to UV radiation. Further, spherical nanoparticles, such a nanosilica, were observed to release during exposure to UV radiation (24,25), but no evidence of fibrous carbon nanotube (CNT) release was observed even after prolonged exposure (26,27). Although nanoparticle released by UV exposure has been detected, the amount of release as a function of exposure has not been measured. There are three main reasons for the lack of quantitative data on nanoparticle release by weathering-induced matrix degradation: 1) the amount of release is very small and, under normal exposure, takes a long time, 2) the lack of high intensity accelerated weathering device to cause significant polymer degradation within a reasonable time, and 3) lack of methodologies for detecting, capturing and quantifying released nanoparticles.

The main objective of this study is to develop protocols and methodologies for measuring the amount of nanoparticles released during the exposure of polymer nanocoatings to an UV environment. Specimens of an epoxy coating containing silica nanoparticles were exposed to a well-controlled, accelerated UV environment, and the amount of nanosilica release as a function of UV exposure was measured by a highly mass-sensitive spectrometric method. Chemical degradation, mass loss, and nanocoating surface morphological changes were also tracked. The results showed that after exposure to 295 nm to 400 nm UV radiation, the epoxy polymer

underwent photodegradation, exposing a large concentration of silica nanoparticles on the surface and releasing a substantial amount of nanosilica.

This result is the first set of quantitative data reported on nanosilica release from nanocoatings that have been exposed to UV radiation with a wavelength range similar to that of ground level sunlight. These data are valuable for developing a model to predict the long term release of nanosilica from polymer nanocomposites and their coatings when used outdoors. Furthermore, the protocols and methodologies advanced in this study for quantifying the amount of nanoparticle release should be helpful for developing standard methods to measure nanoparticle release by weathering. Despite the important implications of the nanoparticle release during the life cycle of polymer nanocomposites and their coatings, such quantitative methodologies currently do not exist. Lastly, surface accumulation and release of silica nanoparticles during UV exposure of its composites may be of a concern, because this nanomaterial has shown a harmful effect to human and the environment (9, 11). Appropriate methodologies and standards should be developed to mitigate and manage the potential risks.

EXPERIMENTAL PROCEDURES

Materials and Preparation of Nanocoating

The silica nanoparticles (i.e., nanosilica) were an untreated, pure material, having an average primary diameter of 15 nm and purity greater than 99.5 %. The epoxy coating was a model stoichiometric mixture of a diglycidyl ether of bisphenol A (DGEBA) epoxy resin with an equivalent mass of 189 (grams of resin containing one gram equivalent of epoxide) and a tri-polyetheramine curing agent. There were no UV stabilizers added to the amine-cured epoxy coating. It should be noted that, due to steric hindrance and restricted transport during the late curing stages, some residual unreacted epoxide and amino groups are expected to be present in the coating films after curing. The presence of these functional groups and impurities (e.g., residual catalysts, processing aids) may have an influence on the photodegradation of an amine-cured epoxy coating. The solvent used for

nanoparticle dispersion and coating processing was reagent grade toluene (purity > 99.5 %). The chemical structures of the components and the cured epoxy coating are given elsewhere (24).

Free-standing films of the amine-cured epoxy containing 5 % mass fraction of nanosilica with a thickness between 125 μm and 150 μm (measured by a caliper) were prepared following the procedure described in Ref. (24). Briefly, silica nanoparticles were first sonicated in a large amount of toluene (5 g of nanosilica in 100 mL of toluene) for 90 min using a 50 kHz tip sonicator (the use of a large amount of solvent is critical for obtaining a reasonable dispersion of untreated nanosilica in the epoxy polymer). After adding the appropriate amount of the epoxy resin, the nanosilica suspension was sonicated for an additional 2 h. The amine curing agent was then added to the suspension, and the mixture was sonicated for another hour followed by stirring for another 30 min with a mechanical stirrer. For comparison, neat epoxy (no nanosilica) films having similar thickness were also prepared by mixing the appropriate amounts of amine curing agent and epoxy resin followed by stirring only with a mechanical stirrer. After the mixing step, mixtures were degassed under vacuum for 30 min at room temperature and then drawn down on a polyethylene terephthalate sheet (a good release substrate for epoxy-base materials). All films were cured at ambient conditions (24 °C and 50 % relative humidity) for 1 day, followed by post-curing for 45 min at 110 °C in an air circulating oven. The post-cure temperature was above the glass transition temperature, T_g, of the cured film, which was measured to be 102 ^{o}C $\pm$ 2 ^{o}C (by dynamic mechanical analysis), to attain maximum curing. The quality of all neat amine-cured epoxy and silica nanocoatings was good with no evidence of air bubbles or defects. In addition, thin films of both neat epoxy and nanocoating having a thickness of 7 μm were also prepared on a CaF_2 substrate for studying degradation using transmission Fourier transform infrared spectroscopy. Hereafter, the neat amine-cured epoxy coating and amine-cured epoxy coating containing 5 % mass fraction of untreated nanosilica are designated as neat epoxy and nanocoating, respectively.

UV Exposure

Specimens of neat epoxy and nanocoating in special holders (Figure 1) were exposed to 60 $^{\circ}$C/0 % relative humidity (RH) conditions in the National Institute of Standards and Technology(NIST) 2 m integrating sphere-based weathering chamber, referred to as SPHERE (Simulated Photodegradation *via* High Energy Radiant Exposure), which is described in detail elsewhere (28). The SPHERE UV chamber utilizes a mercury arc lamp system that produces a collimated and highly uniform UV flux of approximately 140 W/m^2 in the 295 nm to 400 nm wavelength. It can precisely control the relative humidity and temperature within the sample exposure chamber. Because the visible and infrared radiation of the UV source had been removed, the ambient temperature in a SPHERE UV sample chamber is about 27 $^{\circ}$C ± 2 $^{\circ}$C. Thus, an external heat source was used to increase the temperature to 60 $^{\circ}$C to accelerate the chemical degradation process. The very dry conditions were used to minimize any effect of water on the photodegradation of amine-cured epoxy.

a   **b**
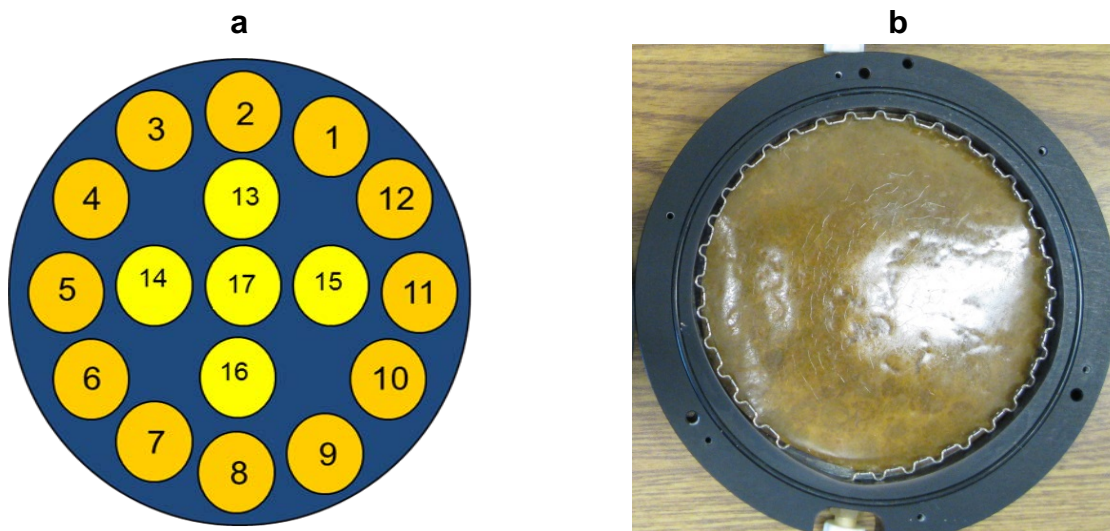

Figure 1. a) 17-window sample holder used to expose specimens to UV for various characterizations, and b) a photograph of a holder containing an UV-exposed nanocoating specimen used for nanosilica release measurement.

Except for studying nanosilica release where a larger size was used, specimens for other characterizations of neat epoxy and nanocoating having a dimension of 25 mm x 25 mm were first mounted in a 17-window sample holder (Figure 1a). Specimens

were removed after specified accumulated UV doses (i.e., at specified time intervals) for various characterizations. Dose, in MJ/m^2, is defined here as the total accumulated energy resulting from repeated UV radiation exposures at a particular time period per unit irradiated surface. Because the SPHERE was operated continuously during this experiment, its UV dose is linearly proportional to the exposure time.

Measurement of Nanosilica Release

For the nanosilica release measurements, nanocoating specimens having a 10 cm diameter were fitted in a specially-designed sample holder (Figure 1b), and the amount of nanosilica released as a function of UV dose were measured as silicon (Si) by an inductively coupled plasma-optical emission spectrometry (ICP-OES) technique. ICP-OES is a multi-element analysis technique that uses inductively coupled plasma to vaporize the samples and then excite the atoms and/or ions of the samples. The detection limit of ICP-OES for Si is ≈ 5 μg/kg. The procedure for collecting released nanoparticles is schematically illustrated in Figure 2. At a specified UV dose (i.e., each exposure time interval), the 10 cm diameter specimen was removed from the closed holder, placed perpendicular to the horizontal surface, and the UV-exposed surface was sprayed with de-ionized (DI) water using a chromatographic atomizer. The runoff water after each spraying was collected in polyethylene bottles for ICP-OES analysis. To optimize the reproducibility of the spraying operation and the collection of nanosilica released after each UV dose, the spraying was performed using the following methodology, which was used for all sprayings: a 10 min spraying time, a 10 cm distance between the atomizer and the specimen surface, and the same atomizing air pressure (around 12 psi or 83 kPa) that resulted from a constant flow rate of 16 L/min. A volume of approximately 25 mL of water was collected for each 10 min spraying. After spraying, the specimens were placed back in their respective holders for further UV exposure. The water spraying simulates rain when exposure outdoors. Three nanocoating specimens were used for each UV dose.
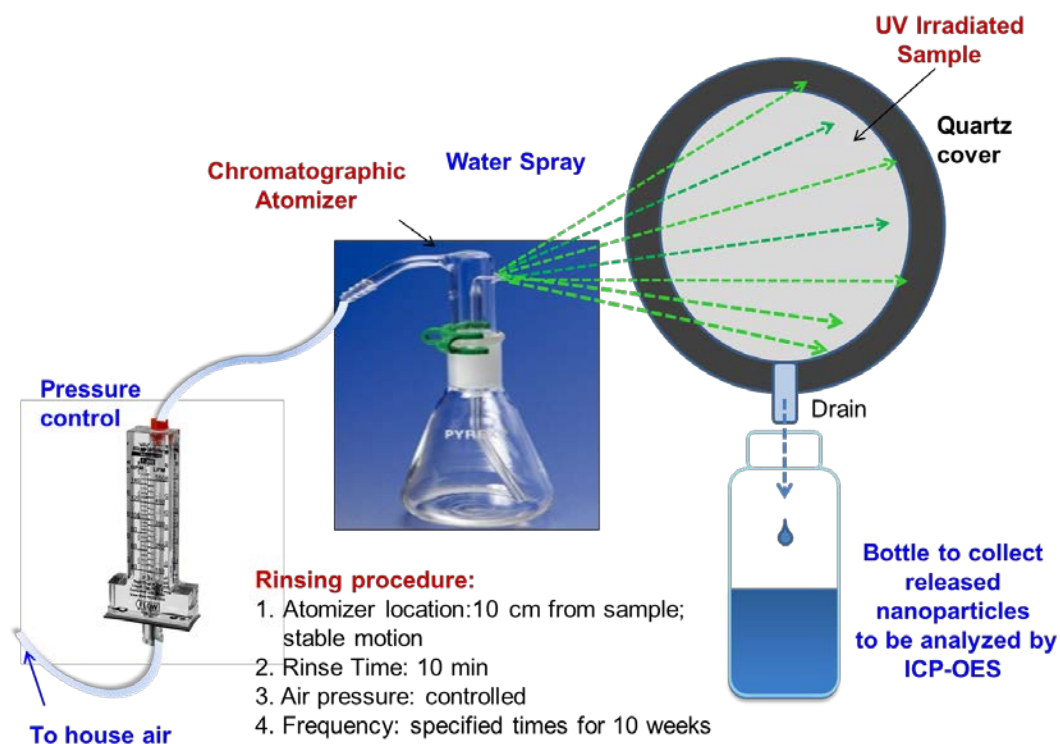
Figure 2. A schematic of the spraying methodology used to collect nanosilica released from epoxy nanocoatings that had been exposed to UV radiation.

ICP-OES analyses of the Si released from the UV exposed nanocoatings were performed using a PerkinElmer Optima 5300 DV instrument (Shelton, CT). The method of standard additions was used to quantify the mass of Si release. Each runoff water sample collected in the bottle was split into two solutions and one solution was spiked with Si. The spiked stock solution contained 9 μg/g Si, prepared from the SRM 3150 Silicon Standard Solution (Lot# 071204). A 0.5 g aliquot was taken from the Si spiked stock solution and added to a 5 g sample solution. Phosphorus was used as an internal standard at a concentration of 1 μg/g. The Si mass fractions in the solution samples were measured according to the parameters in Table 1. Five replicates comprised each measurement, and each solution was measured at two different times.

Table 1: Operating conditions for ICP-OES

Power (kW)	1.5
Plasma gas (L/min)	15
Auxiliary gas (L/min)	0.5
Nebulizer gas (L/min)	0.6
Nebulizer	MiraMist
Spray chamber	Cyclone
Viewing	Axial
Sample uptake	0.7
Analyte wavelength	Si I 251.611
Reference wavelength	P I 213.617
On-chip integration time	0.512
Total read time (s)	8.192

Characterizations of Nanocoating Degradation

Chemical degradation, mass loss, and changes in surface morphology due to UV exposures of neat epoxy and/or nanocoating were characterized. The chemical degradation of both neat epoxy and nanocoating was measured using attenuated total reflection Fourier transform infrared spectroscopy (ATR-FTIR), X-ray photoelectron spectroscopy (XPS), and UV-visible spectroscopy (UV-Vis). ATR-FTIR spectra were recorded at a resolution of 4 cm^{-1} using dry air as a purge gas and a spectrometer (Nexus 670, Thermo Nicolet) equipped with a liquid nitrogen-cooled mercury cadmium telluride (MCT) detector. A ZnSe prism and 45° incident angle were used for the ATR-FTIR measurement. All spectra were the average of 128 scans. The peak height was used to represent the infrared intensity, which is expressed in absorbance, A. All ATR-FTIR results were the average of four specimens. UV-Visible spectra were recorded using an HP 8452A spectrometer fitted with an autosampler. It measures wavelengths from 190 nm to 1100 nm with an integration time of 0.5 s.

XPS analyses were carried out using an Axis Ultra DLD spectrophotomer (Kratos Analytical) equipped with a monochromated Al Kα X-ray source (1486.6 eV). The photoelectrons were collected along the surface normal at a pass energy 40 eV and a step size of 0.1 eV/step for the C(1s), Si(2p), O(1s) and N(1s) regions. All XPS spectra were fit with a Shirley baseline, and adjusted with the appropriate elemental sensitivity factors to obtain information on percent composition. Surface morphological changes of nanocoating were followed by tapping mode atomic force microscopy (AFM) at ambient conditions (24 $^{\circ}$C, 50 % relative humidity) using a Dimension 3100 system (Veeco Metrology) and silicon probes (TESP 70, Veeco Metrology). Both topographic (height) and phase images were obtained simultaneously using a resonance frequency of approximately 300 kHz for the probe oscillation and a free-oscillation amplitude of 62 nm ± 2 nm. The mass loss was determined using an analytical balance having a resolution of 10^{-5} g.

RESULTS

Chemical Degradation of Nanocoating Exposed to UV

Fourier Transform Infrared Spectroscopy (FTIR) Analysis

ATR-FTIR difference spectroscopy was used to follow chemical degradation of both neat epoxy and nanocoating as a function of UV dose. Although raw FTIR spectra recorded at different UV doses (or times) can provide some information about chemical changes in a polymeric material, its degradation is better studied using difference spectroscopy, where the gain or loss of a particular functional group can be readily discerned. The probing depth of the ATR technique is a function of the incident angle, wavelength, and refractive indices of both the prism and the polymer. For the ZnSe prism and 45° incident angle used in this study, the probing depth in the epoxy polymer (refractive index 1.5) in the infrared region of 800 cm^{-1} to 3600 cm^{-1}, as calculated by the internal reflection penetration depth equation (29) is between 0.5 μm and 2.5 μm from the surface. The probing depth in a silica material (refractive index 1.46) is slightly greater than that in the epoxy polymer.

Because the refractive index of a composite is the average of that of the polymer and the filler, the inclusion of only a 5 % mass fraction of silica nanoparticles in the epoxy has a very small effect on its refractive index. Therefore, any chemical change in the nanocoating resulting from UV exposure as detected by ATR-FTIR is essentially similar to that of the neat epoxy; that is, within 2.5 µm of the surface.

Figure 3 shows difference ATR-FTIR spectra of the neat epoxy and nanocoating taken at different UV doses. These spectra were obtained by subtracting the spectrum of the unexposed specimen from those recorded at different doses on the same specimen after normalizing to a reference band (1380 cm^{-1}, due to the gem-dimethyl CH$_3$) to account for any effect due to sampling. Normalization is essential for study of polymer degradation by the ATR technique because, as the degradation becomes more severe, the surface becomes rougher and stiffer, which affects the ATR intensity. Data about the behavior of the 1380 cm^{-1} band with UV exposure was obtained from a parallel quantitative transmission FTIR study of a thin (7 µm) spin casting film on a CaF$_2$ substrate. The intensity of this 1380 cm^{-1} band (not shown) in the transmission spectrum showed little change up to 340 MJ/m^2 dose. In a difference spectrum, bands below and above the zero absorbance line represent a loss (e.g., chain scission) and a gain (e.g., oxidation), respectively, of a functional group in the sample.
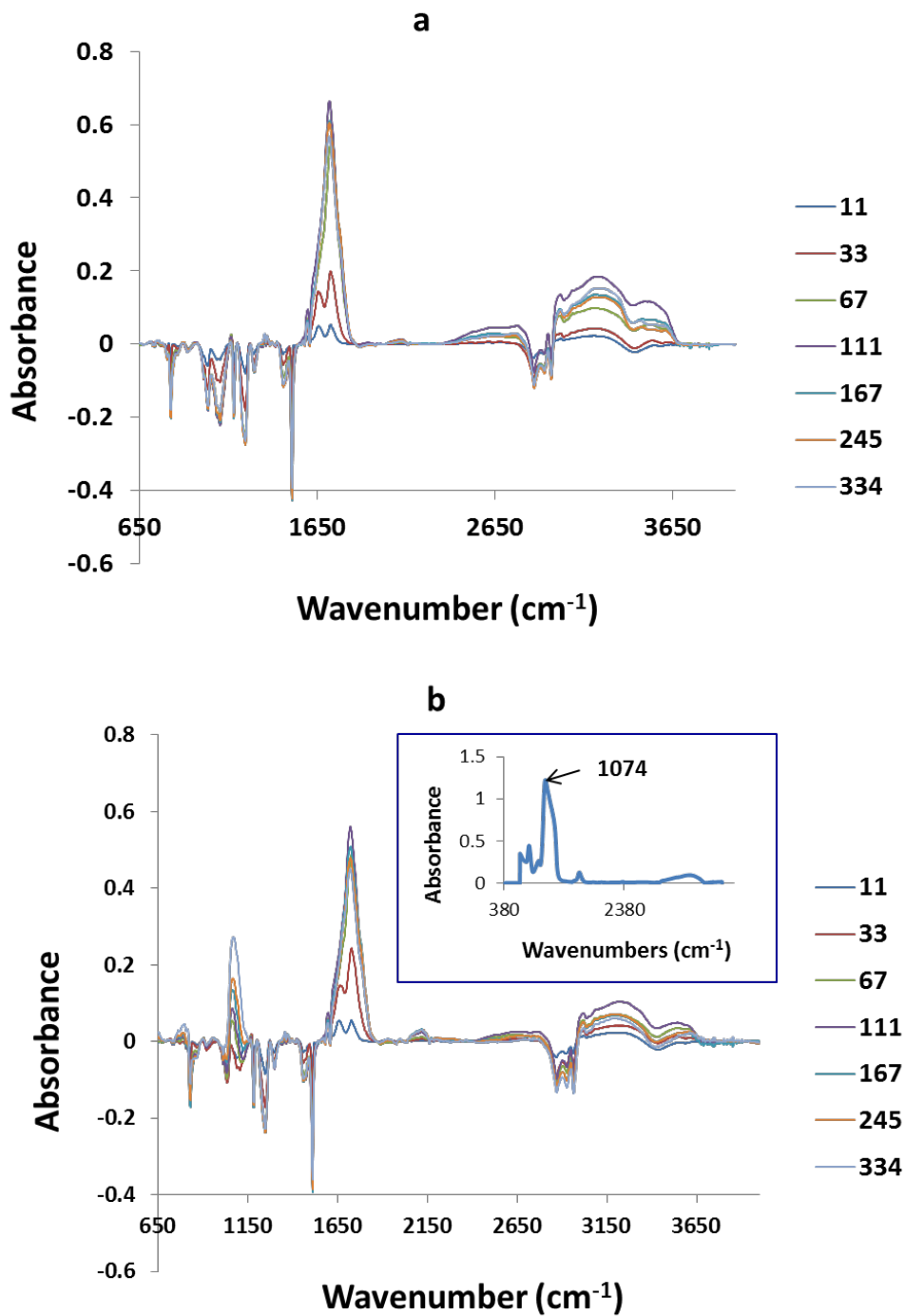
Figure 3. Difference ATR-FTIR spectra of (a) neat epoxy and (b) nanocoating at different UV doses. The inset is a transmission FTIR spectrum of the pure, untreated silica nanoparticles. The number corresponding to each colored line in the right column is the UV dose [MJ/m^2].

Figure 3 shows that, except for the 1000 cm^{-1} to 1200 cm^{-1} region, the spectral changes between the neat epoxy and the nanocoating are similar. That is, the intensities of numerous bands of the epoxy structure substantially decreased under UV radiation, including the bands at 1508 cm^{-1} due to the benzene ring, 1245 cm^{-1} due to aromatic C-O. New bands appeared in the 1620 cm^{-1} to 1740 cm^{-1} region attributed to C=C formation and various carbonyl groups (C=O), such as aldehydes, acids, ketones, and amides. The appearance of these bands is similar to the mechanism proposed previously for DGEBA epoxy resin cured with amines (30-33). The degradation is believed to be through a photo-oxidation process, in which the free radicals generated by chromophoric impurities initiate the photodegradation by the abstraction of hydrogen from the polymer chains, leading to extensive chain scissions, oxidation, and crosslinking. Ketone formation is derived from the secondary hydroxyl groups, while amide is generated from the abstraction of a hydrogen atom from the methylene groups adjacent to the crosslink. The photochemical degradation processes lead to a loss of performance in the epoxy composites, such as a decrease in mechanical properties, yellowing, and cracking. Carbonyl groups can absorb radiation at long wavelengths and, therefore, can accelerate the degradation. Previous studies have shown that photodegradation of amine-cured epoxy coatings is a localized, inhomogeneous process (34), and UV radiation is the main factor that causes the degradation while moisture plays a minor role (35).

To assign the chemical groups responsible for the increase in the 1000 cm^{-1} to 1200 cm^{-1} region with UV dose for the nanocoating (Figure 3b), we recorded a transmission FTIR spectrum of a KBr disc containing untreated silica nanoparticles (Figure 3b inset). It shows, among two other minor bands, a broad strong band near 1074 cm^{-1}, assigned to the Si-O-Si bonds (36). Based on this result, the intensity increase in the 1000 cm^{-1} to 1200 cm^{-1} region with increasing UV exposure for the nanocoating is attributed to the increase of silica nanoparticles on the surface. It is noted that the epoxy structure also contains various C-O bands in the 1000 cm^{-1}-1200 cm^{-1} region, but these bands decrease with UV exposure. Therefore, the intensity increase in the 1000 cm^{-1} to 1200 cm^{-1} region observed in Figure 3b is actually an underestimate of the concentration of nanosilica detected. Figure 3 also showed an intensity increase with UV dose in the 3050 cm^{-1} to 3500 cm^{-1} region for

both neat epoxy and nanocoating, suggesting the formation of OH (from carboxylic acids) and NH groups.

The bands at 1245 cm^{-1} and 1724 cm^{-1}, represent chain scission and oxidation of the epoxy. And the band at 1060 cm^{-1} is attributed to epoxy C-O and Si-O bonds. These three bands were used to follow various degradation processes and surface accumulation of silica nanoparticles of nanocoating during UV exposure. Intensity changes of these bands after normalization to 1380 cm^{-1} with UV dose are displayed in Figure 4. The error bars in Figure 4 indicate a good reproducibility between specimens. As seen in Figure 4, both neat epoxy and nanocoating underwent rapid photodegradation with extensive chain scission and formation of a substantial amount of oxidized products under UV exposure. The rates of both chain scission and oxidation were rapid between 0 MJ/m^2 and approximately 130 MJ/m^2 but leveled off thereafter. Similar rapid degradation/oxidation followed by a leveling off was also observed for the same intensity vs. dose curves obtained by transmission FTIR on 7 μm films. The leveling off in chemical degradation is generally attributed to the depletion of degradable functional groups in the polymer.

Figure 4 also reveals that both chain scission and oxidation in the neat epoxy were similar to those in the nanocoating at low doses (≤ 40 MJ/m^2), but these degradation modes for the nanocoating were lower than those of the neat epoxy at high doses. The lower intensity values for the nanocoating are attributed to the accumulation of nanosilica on the nanocoating surface as a result of UV exposure. As seen later in the section on surface morphological changes, silica nanoparticles increasingly accumulated on the UV-exposed nanocoating surface with exposure time. The presence of the nanoparticles on the surface likely decreased the amount of UV radiation penetrating into the nanocoating, hence less degradation. An examination of intensity changes in the transmission FTIR spectra (not shown) for the 7 μm specimens exposed to the same UV conditions revealed that both chain scission and oxidation of the two materials were essentially similar, suggesting that the untreated nanosilica neither catalyzed nor photo-stabilized this amine-cure epoxy coating.

The increase of silica materials on the nanocoating surface is confirmed chemically by the results in Figure 4c, which displays the intensity changes of the 1060 cm^{-1} band (attributed to the combined C-O and Si-O bonds) with UV dose. The intensity of this band for the nanocoating rose but that of the neat epoxy decreased with UV dose; the latter behavior is similar to other bands of the epoxy resin. The increase of this band is believed to be due to the increase of the nanosilica concentration on the nanocoating surface during UV exposure. However, because the total intensity of the 1060 cm^{-1} band is the combination of the C-O and Si-O bonds, the actual increase in the intensity, which represents the total concentration of nanosilica detected by ATR-FTIR, is the sum of the C-O intensity decrease in the neat epoxy and the nanocoating intensity values shown in Figure 4c.
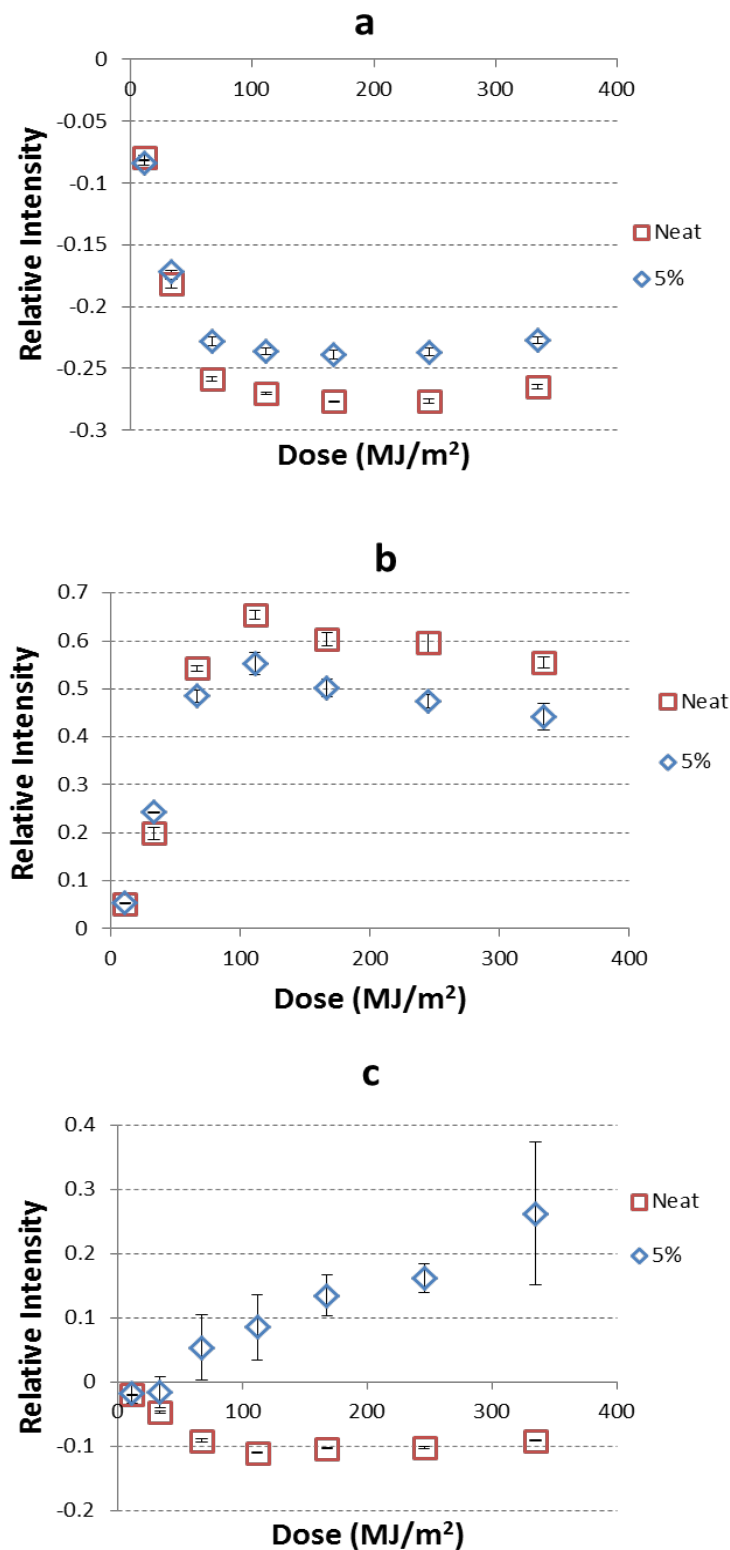
Figure 4. ATR-FTIR intensity changes with UV dose for the following bands: a) 1245 cm^{-1}, b) 1724 cm^{-1}, and c) 1060 cm^{-1} for neat epoxy and nanocoating. The intensities have been normalized to that of the band at 1380 cm^{-1}. The results are the average of 6 specimens, and error bars represent one standard deviation.

UV-visible Spectroscopy Analysis

Chemical changes in the neat epoxy and the nanocoating are also observed by UV-visible spectroscopy, as displayed in Figure 5. Figures 5a and 5b display the UV-visible spectra of neat epoxy and nanocoating, respectively, taken at different UV doses, and Figure 5c illustrates the intensity vs. dose curves at 354 nm for the two materials. The unexposed neat epoxy (Figure 5a) has little absorption beyond 300 nm, but the same material containing a 5 % mass fraction of untreated nanosilica (Figure 5b) had a considerable absorption between 300 nm and 450 nm and a smaller absorption between 450 nm and 700 nm. This could be due to aggregation of silica nanoparticles. Under UV irradiation, the UV-visible absorption increased significantly between 0 MJ/m^2 and 175 MJ/m^2 (around 14 d), but subsequent absorption after similar additional exposure increased much less, in good agreement with FTIR results on oxidation and chain scission shown in Figure 4c. These results suggest that a substantial amount of double bond compounds have been formed in both materials due to UV exposure, and that a substantial color change (yellowing) has occurred in both materials. Indeed, we observed that both neat epoxy and nanocoating became more yellow with increasing dose. At the highest dose, both materials had a dark brown color.

Comparing the intensity changes with UV exposure of the two materials, the increase in absorbance was larger for the nanocoating than that for the neat epoxy (Figure 5c). For the neat epoxy, the substantial absorbance increase with UV dose extended from about 250 nm to 500 nm, but that of the nanocoating covered a much wider wavelength range, from a similar low wavelength to a higher wavelength in the visible range (approximately 700 nm). This phenomenon may be related to the increased aggregation that results from a higher amount of nanosilica accumulated on the surface with longer exposure, as seen later in the section on surface morphological changes.
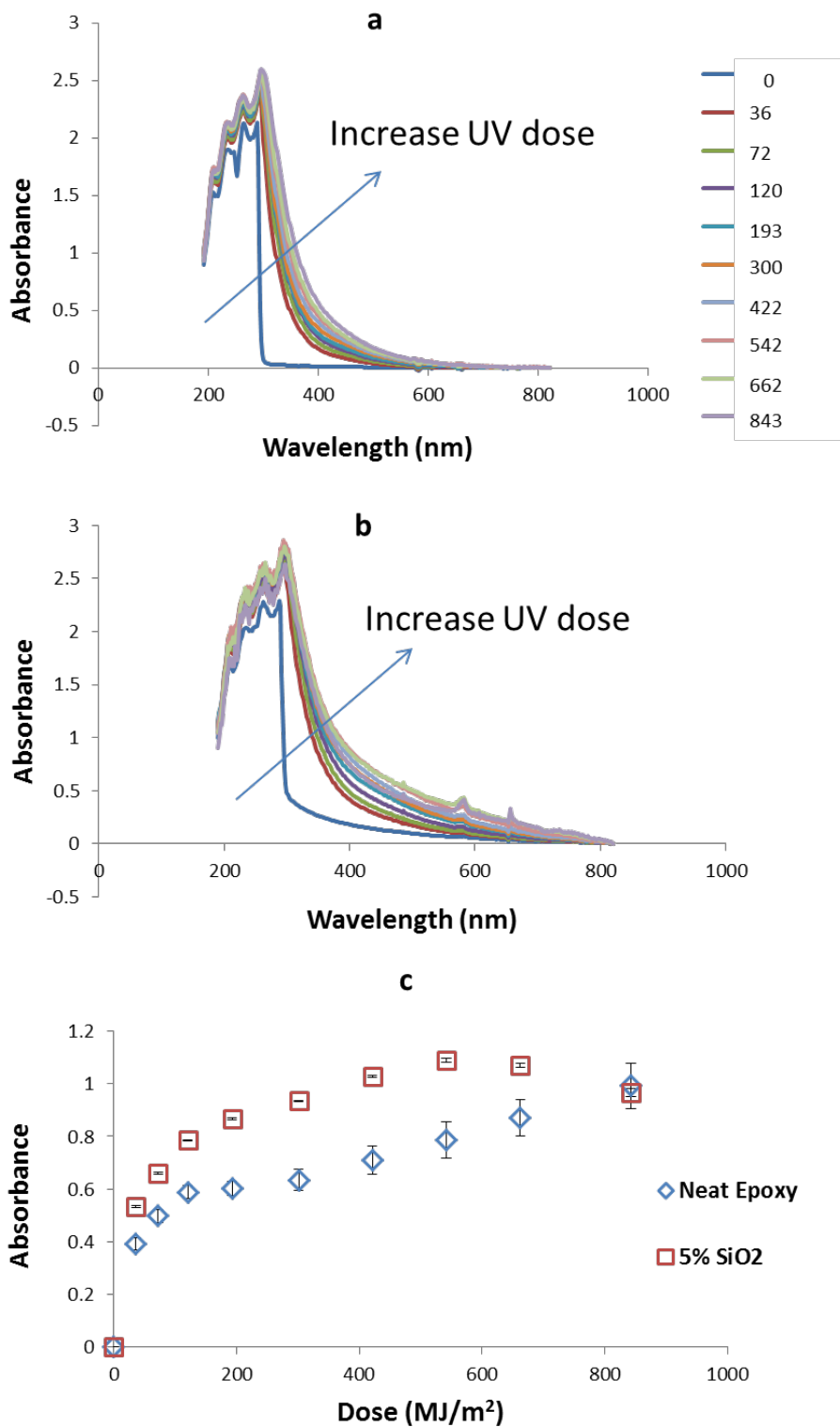
Figure 5. UV-visible spectral changes of neat epoxy and nanocoating as a function of UV dose; a) UV-vis spectra of neat epoxy at different UV doses, b) UV-vis spectra of nanocoating at different UV doses, and c) UV-vis intensity at 354 nm as a function of UV dose for neat epoxy and nanocoating. The results in (c) are average of 4 specimens, and error bars represent one standard deviation. The number corresponding to each colored line in the right column is the UV dose.

The loss of the epoxy matrix and the increase in the silica material near the nanocoating surface as a function of dose as observed by ATR-FTIR in Figure 4 is consistent with the XPS results displayed in Figure 6. As the UV dose increased from 0 MJ/m^2 to 770 MJ/m^2, the percent surface concentrations of carbon decreased from 77.4 % ± 1.4 % to 50.2 % ± 1.7 %, while those of silicon started at 3.4 % ± 0.8 %, dropped after a short dose of 54.1 MJ/m^2 to 0.9 % ± 0.1 % followed by a steady rise to a final value of 6.5 % ± 0.4 %, and nitrogen increased from 1.4 % ± 0.2 % to 8.1 % ± 0.2 %. The increase in nitrogen with UV dose observed in Figure 6 for the untreated nanosilica composite may be explained as due to the adsorption of amine curing agent on the untreated nanosilica surface during mixing and film formation. In this case, the adsorbed amine would form an interfacial layer between the silica nanoparticles and the epoxy polymer. The driving force for the preferential adsorption of amine on silica nanoparticles, instead of epoxy molecule, is the formation of a strong bond between the base amine and the acidic silica through the an acid-base interaction. This is because the Si-OH on the silica surface is a strong proton donor group, which interacts strongly with strong proton acceptor NH through the formation of a SiO$^{-}\cdots$NH$_3^+$ complex. The preferential adsorption of amine on silica substrates has been observed for epoxy/glass fiber composites (37), which showed that the amine curing agents from the epoxy mixture migrate from the interior and preferentially adsorb at the glass fiber surface during processing, creating an amine-rich layer on the glass surface that has strong effect on the durability of epoxy/glass fiber composites.
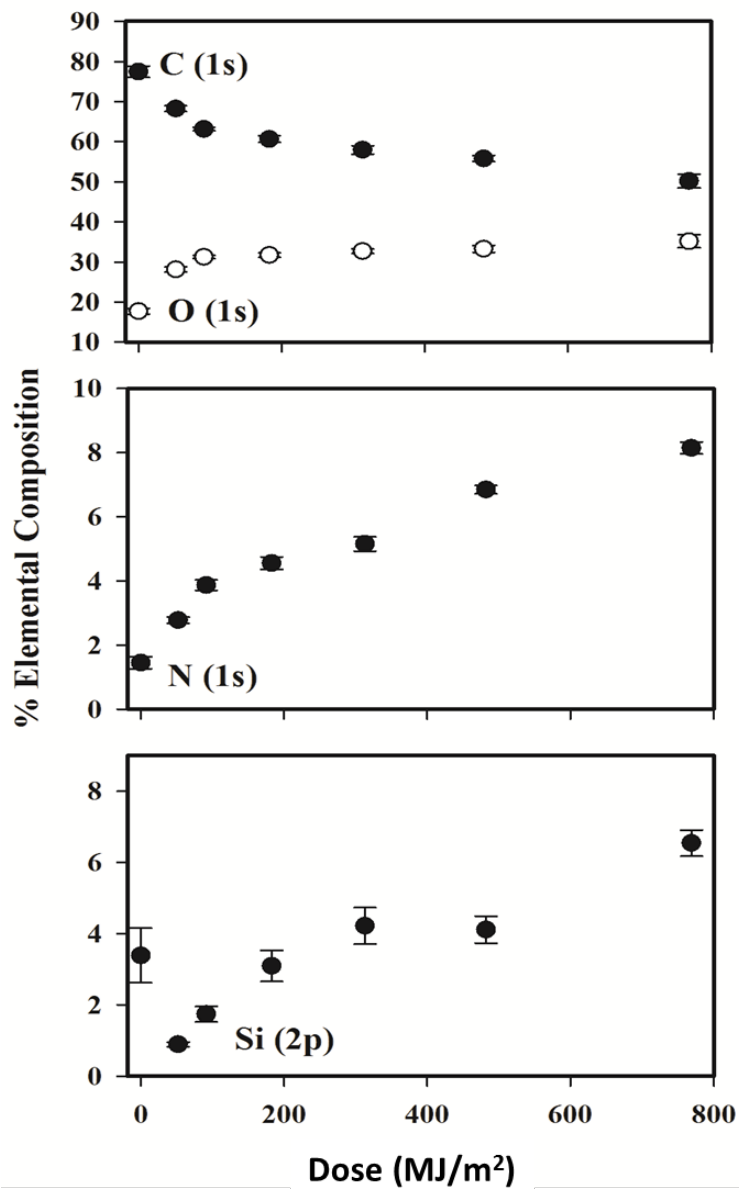
Figure 6. XPS-based carbon (C), oxygen(O), nitrogen(N), and silicon(Si) atomic percentages on the epoxy/nanosilica coatings surface vs. UV irradiation dose. Each data point consisted of two or more specimens and the error bars represent one standard deviation.

Mass Loss

Chemical degradation of the matrix will cause a loss of mass in neat epoxy and nanocoating, and the results as a function of UV dose are displayed in Figure 7. The mass loss is expressed as [(initial mass – mass at any UV dose)/initial mass] x 100. Both materials lost mass rapidly between 0 MJ/m^2 and approximately 400 MJ/m^2 but slowed down thereafter, a similar trend to that of the chemical degradation as shown

in Figure 4a but the slowing down occurred at higher UV doses for the mass loss. This is because the chemical degradation was studied at or near the surface, but mass loss was measured based on thick films. Both the rate and the amount of mass loss of the nanocoating were slightly higher than those of the neat epoxy. The average mass losses for neat epoxy and nanocoating were 1 % and 1.55 %, respectively, after 700 MJ/m^2. The higher mass loss in the nanocoating suggests both the epoxy matrix and higher density silica nanoparticles were removed from the specimens during UV exposure.
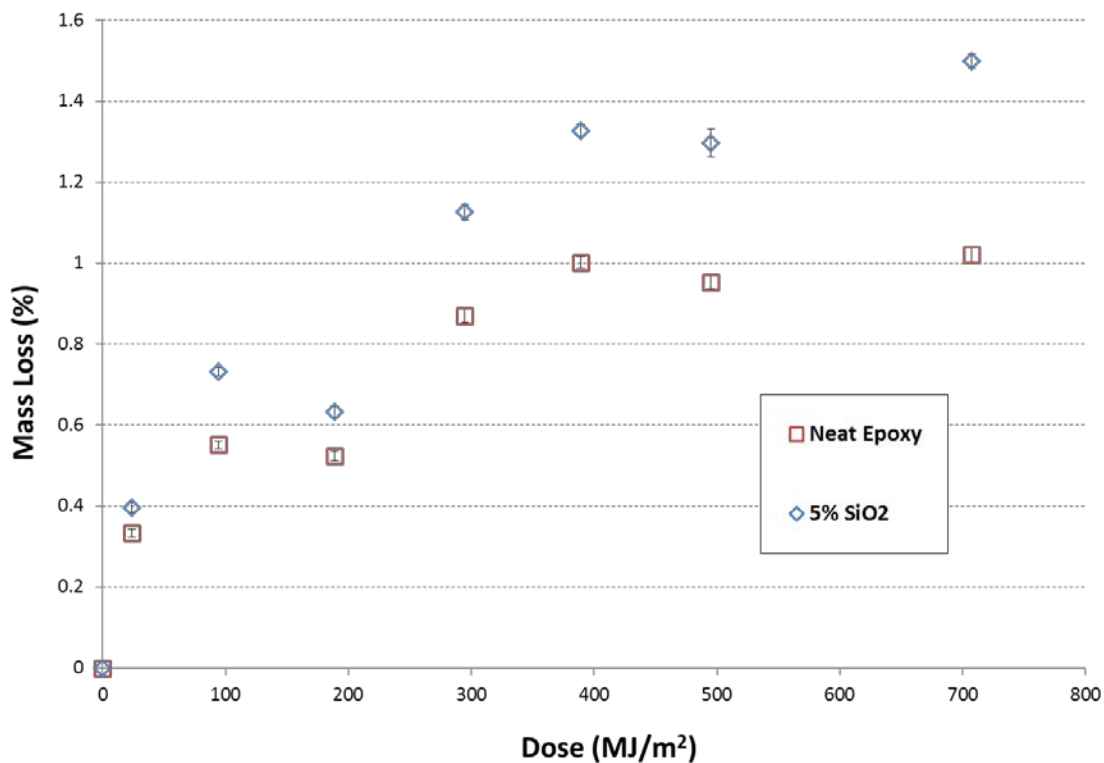

Figure 7. Mass loss of neat epoxy and nanocoating specimens as a function of UV dose. Each data point is the average of 6 specimens, and error bar represents one standard deviation.

Surface Morphological Changes in Nanocoating

Chemical degradation of the matrix in a polymer nanocomposite would expose nanoparticles on its surface during UV exposure, as reported previously (24,25). In this study, we have employed tapping mode AFM to follow the surface morphological

changes and the kinetics of nanosilica accumulation on the nanocoating surface during UV exposure. In addition to the advantages of scanning the sample at ambient condition and very low applied force, which minimizes damage to the fragile degraded sample surfaces, the phase change of the oscillation during scanning in tapping mode is sensitive to variations in material properties, particularly mechanical properties. Because the modulus of silica is much greater than that of an amine-cured epoxy (73 GPa for silica vs. 1 GPa to 2 GPa for epoxies), the contrast between silica nanoparticles can be readily discerned from the epoxy matrix in an AFM phase image.

Changes in the nanocoating surface with UV exposure are displayed in Figure 8, which shows the height and phase AFM images at two magnifications for various UV doses. The unexposed surface appeared smooth with little evidence of nanoparticles (Figure 8, 0 d, 20 μm scan width). The bright nanoscale features in the darker surrounding seen in the 1 μm phase image scan (Figure 8, top row, far right) of the 0 d sample is due to the microstructure of the amine-cured epoxy (34). After a 91 MJ/m^2 dose of UV exposure, some individual and clustered silica nanoparticles were visible on the surface. The brightness of these nanoparticles in the height image (upper row, second from right) indicates that they are raised above the surface. With further exposure, the concentration of nanosilica on the surface continues to increase, and after a 391 MJ/m^2 dose, only silica nanoparticles in the clustered form are observed. After 808 MJ/m^2, a layer of compact nanosilica has covered the entire nanocoating surface. Figure 8 also reveals other features that are of interest. For example, it shows that at high UV dose, nanosilica aggregated and formed a layer on the surface. Further, the lower magnification image at 808 MJ/m^2 dose exhibits several cracks in the nanosilica-rich surface layer, and those cracks appear to originate from a single location. It is not known whether the crack is through the nanosilica-rich layer thickness or only near the surface. In addition, the high magnification images at low UV doses (91 MJ/m^2 and 182 MJ/m^2) suggest that the dispersion of these untreated silica nanoparticles in the amine-cured epoxy was not uniform.
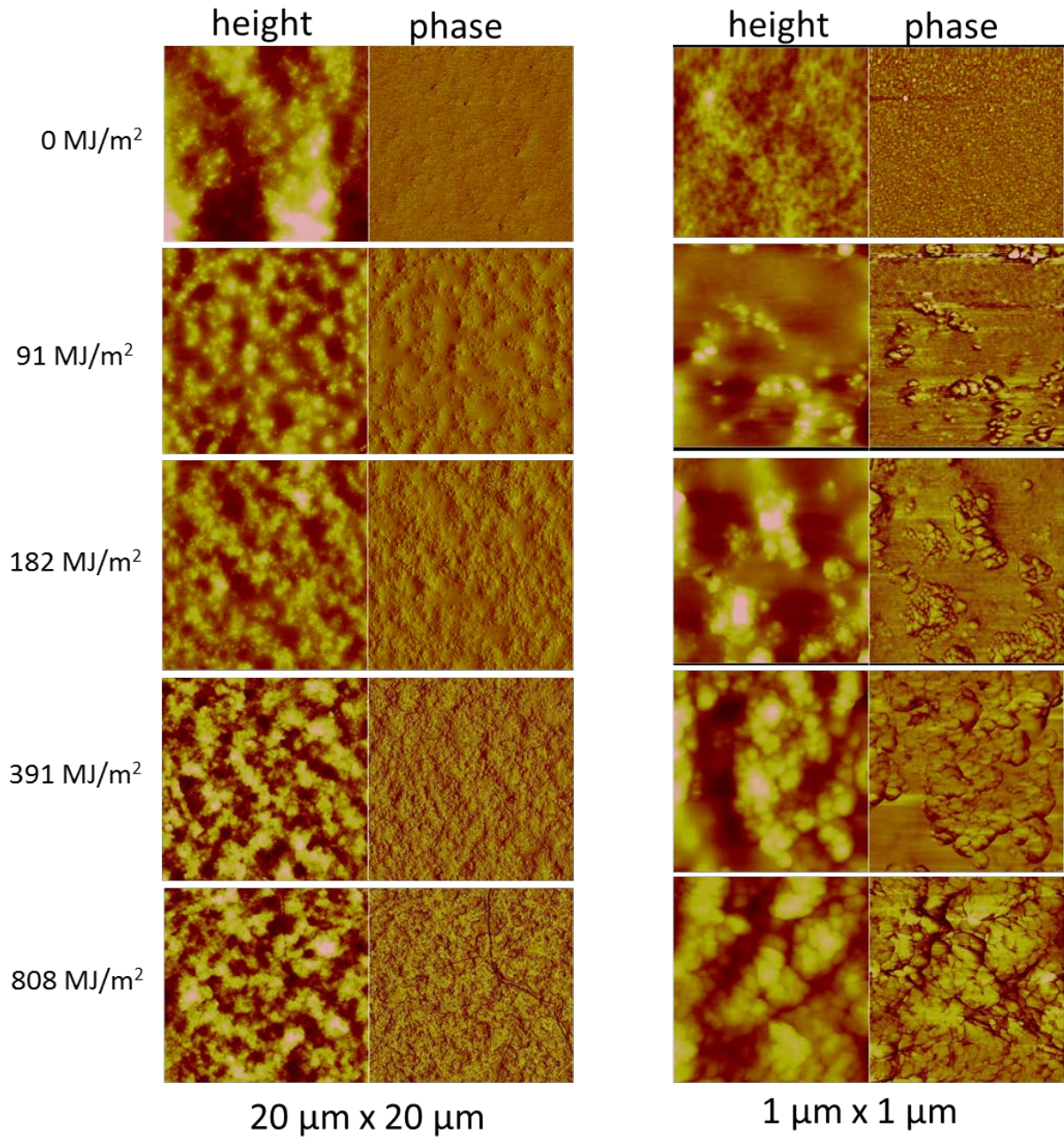
Figure 8. Height and phase AFM images at two magnifications of epoxy/5 % mass fraction nanosilica coating at different UV doses.

Figure 8 also reveals that, although both height and phase imaging AFM are suitable for following the accumulation of nanosilica on the UV irradiated nanocoating surface, the latter imaging mode provides a stronger contrast between the hard inorganic silica nanoparticles and the softer viscoelastic epoxy matrix than that of the former. Because AFM is usually operated at ambient conditions, the results demonstrated that phase imaging AFM is a convenient technique to effectively follow

the accumulation of inorganic nanoparticles on polymer nanocoating surface during exposure to UV radiation.

Applying the image analysis software for height imaging provided by the AFM instrument and carefully adjusting the grey level, we quantified the kinetics of nanosilica accumulation on the nanocoating surface as a function of UV exposure. The results are depicted in Figure 9. It shows that the accumulation of silica nanoparticles on the UV-exposed nanocoating increased rapidly between 0 MJ/m^2 and approximately 400 MJ/m^2, but slowed down thereafter (Figure 9). The shape of nanosilica coverage vs UV dose curve is similar to those of oxidations (e.g., Figures 4b and 5c) and Si increase (Figure 6) with UV dose, suggesting that the accumulation of silica nanoparticles on the nanocoating surface with UV exposure is closely related to photodegradation of the epoxy matrix. That is, as the epoxy layer on the surface degrades and was removed by UV radiation, silica nanoparticles that were embedded in the matrix were increasingly exposed to the nanocoating surface.
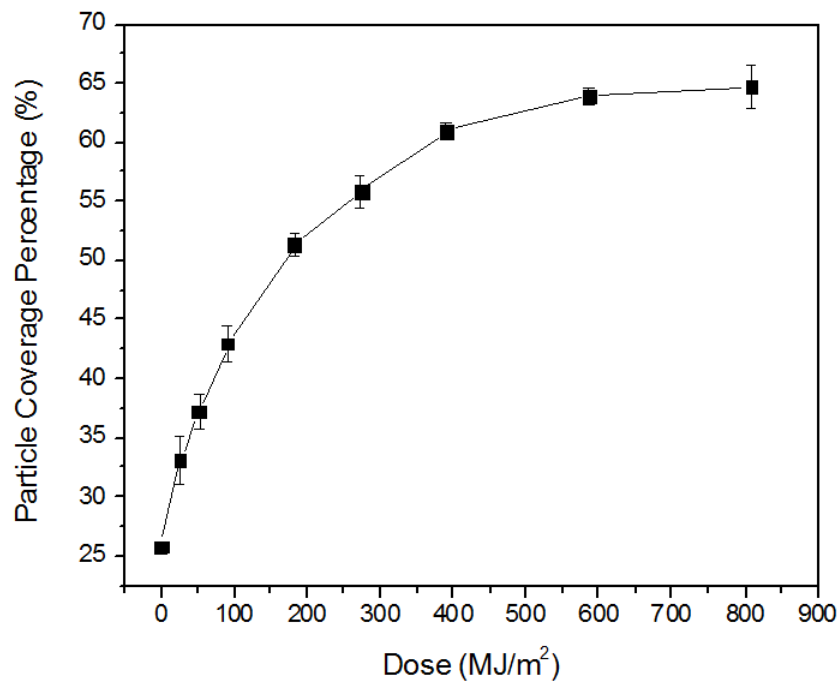

Figure 9. Nanosilica coverage on the nanocoating surface as a function of UV dose. The analysis was based on 20 μm scan height images. Each data point is the average of three images scanned from three different locations; the error bars represent one standard deviation.

Quantifying the Amount of Nanosilica Release from Nanocoating Exposed to UV

As described in the experimental section, UV-exposed nanocoating specimens having 10 cm diameter were sprayed with DI water at a constant pressure for 10 min, and the runoff waters were collected and analyzed by ICP-OES. Table 2 presents the amount of Si collected at different UV doses for two separate specimens, S1 and S2. This table also includes the total amount of Si from a specimen (S3) having the same diameter but was sprayed with water only after exposing to the highest UV dose (end of the experiment). Clearly, periodic water showering during UV exposure had generated more nanosilica release than spraying at the end of the experiment. It should be mentioned that the silica nanoparticles used were a pure, untreated material, and thus the Si values measured in Table 2 are presumed to be solely from the silica nanoparticles that were embedded in the epoxy matrix, and not from the silane coating typically found in the commercial silane-treated nanosilica products.

Table 2 reveals that the runoff water of the unexposed specimen (0 day) contained a small quantity of Si. Similarly, a small amount of Si was collected from the specimens irradiated for 233 MJ/m^2 dose, suggesting that not many silica nanoparticles were released from the nanocoating surface during this exposure. On the other hand, a substantial amount of nanoparticles are clearly visible in the AFM images taken at this exposed dose (Figure 8). This result suggests that at this stage, the silica nanoparticles were still strongly attached to the nanocoating surface and not removed by water spraying. The amounts of Si release became more substantial for specimens exposed to 350 MJ/m^2 or greater, and after an UV dose of 1,217 MJ/m^2, a total amount of Si between 500 µg to 760 µg were released from the nanocoating. This amounted to a loss of 0.5 % silica (SiO$_2$) (from the initial nanosilica quantity) after 1,217 MJ/m^2 or about 0.143 µg/d/cm^2.

Table 2. Mass of Si release, in µg, measured at each specified UV dose for two nanocoating specimens (S1 & S2) sprayed with water periodically, and a third (S3) that was sprayed at the end of the experiment. The uncertainties represent one standard deviation of total 10 measurements (five replicates, and two measurements on each replicates).

UV dose (MJ/m^2)	S1	S2	S3**
0	0.604 ± 0.027	0.691 ± 0.013	0.6282 ± 0.0082
233	0.861 ± 0.004	0.703 ± 0.026	
350	20.12 ± 0.41	3.41 ± 0.12	
450	25.56 ± 0.40	120.9 ± 4.1	
617	237.2 ± 5.7	102.8 ± 1.9	
734	128.4 ± 1.8	39.75 ± 0.16	
967	56.1 ± 1.5	383.0 ± 5.2	
1217	61.40 ± 0.64	98.02 ± 0.91	301.5 ± 2.7
Total	**542.8 ± 6.2**	**759.3 ± 6.9**	**300.9 ± 2.7**

** S3: sprayed only at the end of exposure

There are two important observations about the quantitative nanosilica release data given in Table 2. First, the cumulative release from sample S2 was nearly 150 % of the release from sample S1, and secondly, the quantities of nanosilica release recorded at each specified UV dose are markedly different. The cause of this marked difference, despite the same UV dose, is unknown. Several factors may contribute to the lack of consistency between companion specimens: 1) non-uniform dispersion (agglomerated particles should release more easily than well-dispersed particles), 2) inhomogeneous photodegradation of epoxy coating (oxidized areas are more polar and can interact more strongly with the OH/NH covered nanosilica than with unoxidized areas), and 3) spraying time (the 10 min used in this study may not be sufficient for water to penetrate fully into the particle/polymer interface and between aggregated particles). Further studies are needed to better understand the lack of reproducibility so that better protocols can be developed to more reliably measure the amount of nanoparticle released during the UV exposure of polymer nanocomposites and nanocoatings.

In an attempt to shed some light on the reproducibility problem, we employed laser scanning confocal microscopy (LSCM) and AFM to analyze specimens S1 and S3 after spraying with water at the end of the experiment. The results are presented in Figure 10.
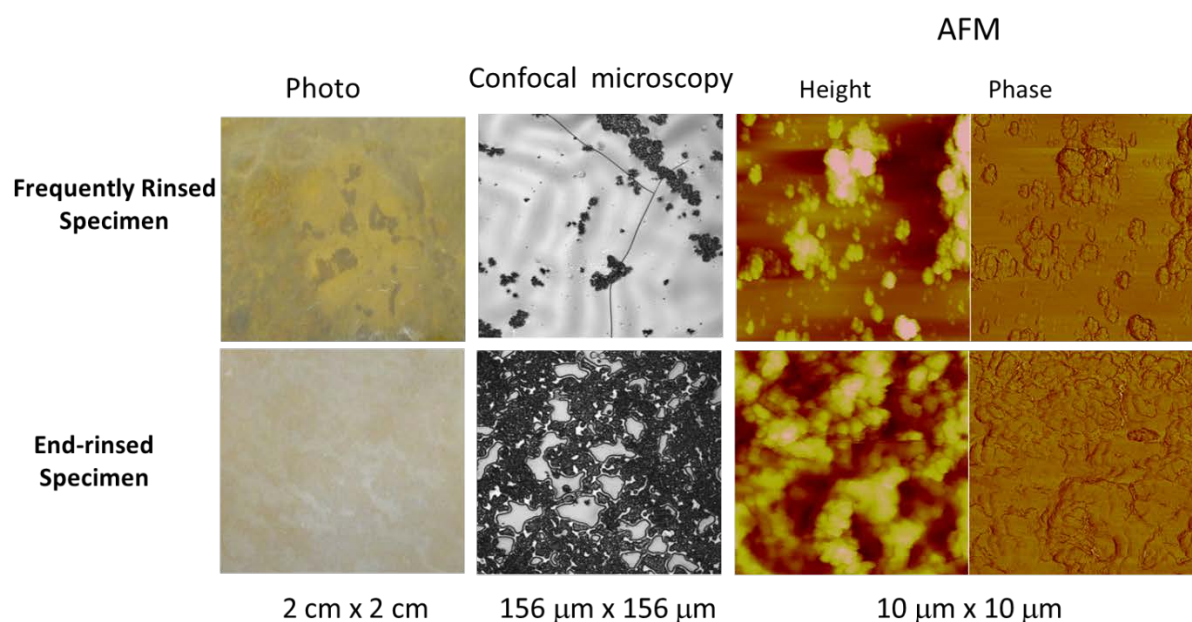

Figure 10. Confocal microscopy and AFM images from nanosilica release specimens exposed to the highest UV dose; top row: frequently sprayed with water, and bottom row: sprayed with water only at the end of the experiment. For each row, the far left image is a picture of the exposed nanocoating.

Figure 10 shows that the particles left on the surface after spraying are highly aggregated. The specimen that was sprayed periodically with water contained fewer particles on the surface than the one sprayed only at the end. This observation is consistent with the results from Table 2; i.e., the specimen that was sprayed periodically with water having more particles released than the one sprayed only at the end. This result suggests that frequently water spraying is a better method for collecting the degradation-induced release of nanoparticles for ICP analysis. The frequently water sprayed specimen also appeared to degrade more severely, as evidenced by the darker color, in good agreement with the higher Si release quantity given in Table 2. Figure 10 also reveals that the removal of nanoparticles by water

spraying from the nanocoating surface was highly non-uniform. Further investigation and additional experiments are ongoing to answer why some surface areas were completely void of particles after spraying while others were still covered with them.

The amount of Si release from the nanocoating as a function of UV dose is depicted in Figure 11. Each data point is the average of the two specimens, S1 and S2. The result for the specimen (S3) sprayed at the end of the experiment (red*) is also included for comparison. Although there are some significant variations between the two replicates, the results show that, after an induction period, the amount of nanosilica release increased with increasing UV dose. It is noted that the release mass vs. dose curve of Figure 11 cannot be compared directly with the nanosilica surface accumulation or chemical oxidation curves, because the specimens for measuring nanosilica release were sprayed with water while those for other measurements were not. As seen in Figure 11, the specimen sprayed frequently with water appeared to degrade faster than that without. As mentioned in the introduction, there have been several reports on the nanoparticle accumulation on the surface of nanocomposites after UV irradiation. However, this set of quantitative data is the first report on nanoparticle release from polymer nanocomposites exposed to UV radiation. This quantitative data is essential for developing models to predict the nanoparticle release rate with UV dose or exposure time to UV, and useful for assessing potential risks of polymer nanocomposites and their coatings used outdoors.
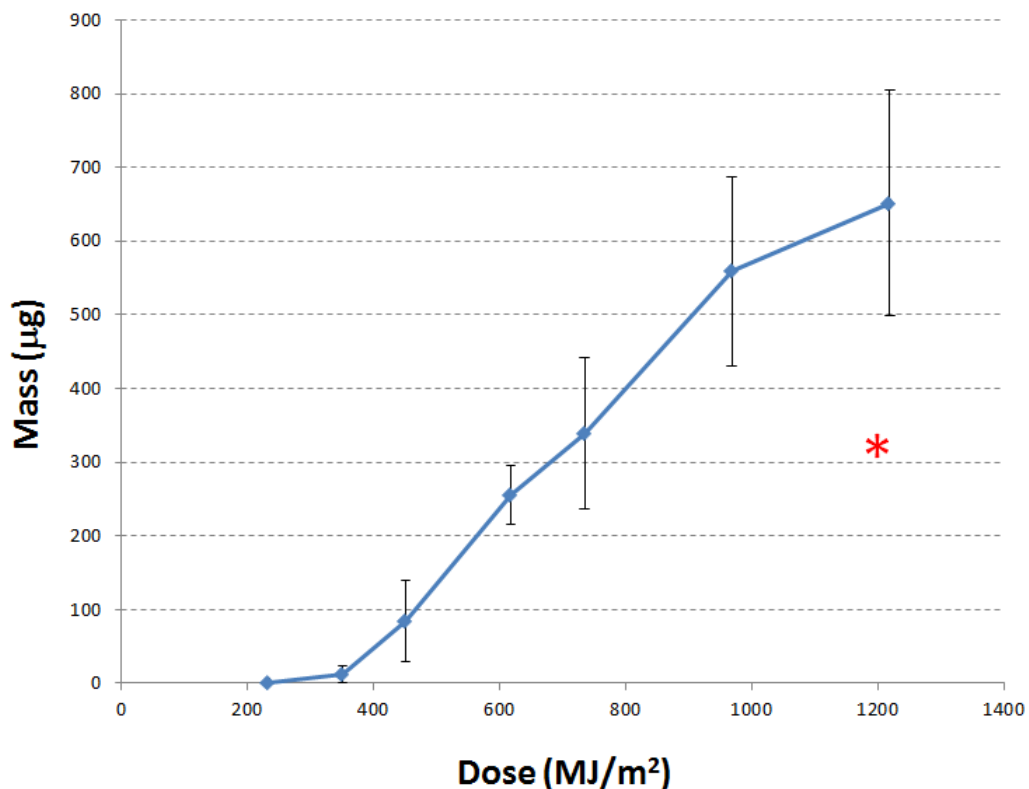
Figure 11. Amount of Si released as a function of UV dose. The results are the average of two 10 cm diameter specimens, and the error bar represents one standard deviation. Red * is the value for the specimen S3 sprayed with water at the end of the experiment.

CONCLUSIONS

Polymer coatings containing nanoparticles are increasingly used in high volume exterior applications. Because polymers are susceptible to degradation by solar UV radiation, nanoparticles in a polymer nanocoating can be released into the environment during their life cycle. Such release raises possible environmental, health and safety concerns that may hinder the commercialization of these advanced materials. This study has investigated a methodology for quantifying the amount of silica nanoparticles released from an amine-cured epoxy nanocoating exposed to UV radiation. Specimens were exposed to a custom-made highly accelerated weathering device, and the amount of released nanosilica was measured as silicon by an inductively coupled plasma-optical emission spectrometry (ICP-OES)

technique. Chemical degradation, mass loss, and surface morphological changes of the nanocoating were also investigated. Based on the results obtained, the following conclusions can be drawn:

1. The epoxy matrix in the nanocoating underwent rapid photodegradation during exposure to 295 nm to 400 nm UV, resulting in a substantial amount of nanosilica accumulated on the surface and subsequently released from the nanocoating. The amount of nanosilica released by periodic water spraying of the exposed specimens was greater than that from an exposed specimen without periodic water spraying.

2. The rate of mass loss of the nanocoating was greater than that of the neat epoxy film, but the rates of chain scission and oxidation near the surface of the former were greater than those of the latter, likely due to the accumulation of nanoparticle on the nanocoating surface.

3. Silica nanoparticles were observed to increasingly accumulate on the nanocoating surface, and the shape of nanosilica coverage vs UV dose curve was similar to those of oxidations observed from FTIR-ATR results (e.g., Figures 4b and 5c) and Si increase from XPS results (Figure 6) with UV dose.

4. A methodology was developed for exposing the nanocoating to UV radiation, collecting the released particles, and quantifying the amount of release by the ICP-OES technique.

5. After an induction period, nanosilica released rapidly from the nanocoating, and the amount of released nanosilica increased with increasing UV dose for frequently rinsed samples.

6. The result of this study is the first set of quantitative data reported on nanosilica release from a nanocoating exposed to UV, and this data is valuable for developing a model to predict the long term release of nanosilica from polymer nanocomposites and their coatings when used outdoors.

7. The protocols and methodologies developed in this study for measuring nanosilica release during UV exposures should be helpful for developing standard test methods for how to conduct weathering experiments to

measure the release of metal oxide nanoparticles from polymer nanocomposites.

8. The observation of a substantial amount of nanosilica accumulated on the surface and released during UV exposure should be useful for assessing the potential risks of polymer nanocomposites and their coatings used outdoors.

Disclaimer

Certain commercial product or equipment is described in this paper in order to specify adequately the experimental procedure. In no case does such identification imply recommendation or endorsement by the National Institute of Standards and Technology, nor does it imply that it is necessarily the best available for the purpose.

References

1. McNally T. and Pötschke P., Eds., Polymer-carbon nanotube composites, preparation, properties, and applications, Woodhead Publishing, Philadelphia, 2011.
2. Potts J.R., Dreyer D.R., Bielawski C.W., and Ruoff, R.S., Graphene-based polymer nanocomposites, Polymer, 52 (2011) 5-25.
3. Pavlidou S. and Papaspyrides C.D., A review on polymer-layered silicate nanocomposites, Progress in Polymer Science, 33 (2008) 1119-1198.
4. Zou, H., Wu, S.S., and J. Shen, J., Polymer/silica nanocomposites: preparation, characterization, properties, and applications, Chemical Reviews, 108 (2008) 3 893-3957.
5. Nanomaterials in plastics and advanced polymers, Market Report # 52, April, 2012, Future Markets, Inc.
6. http://www.researchandmarkets.c/reportinfo.asp?report_id=1824738&t=t
7. Nel, A., Xia, T., Mädler, L, and Li, N., Toxic potential of materials at the nanolevel. Science, 311 (2006): 622-627.
8. Poland C.,et al., Carbon nanotubes introduced into the abdominal cavity of mice show asbestos-like pathogenicity in a pilot study, Nature Nanotechnology, 3 (2008) 423-428.
9. Maynard, A.D., Nanotechnology: assessing the risks, Nanotoday, 2(2006) 22-33.
10. Aschberger, K., et al., Review of carbon nanotubes toxicity and exposure – Appraisal of human health risk assessment based on open literature, Critical Reviews in Toxicology, 40(9) (2010): 759-790.

11. Adams, L. K., Lyon, D.Y., Alvarez, P. J. J., Comparative ecotoxicity of nanoscale TiO_2, SiO_2, and ZnO water suspensions; *Water. Res.*, *40* (2006) 3527–3532.

12. Leem J., Mahendra, S., and Alvarez, P. L., Nanomaterials in the construction Industry: A review of their applications and environmental health and safety considerations, ACSNano, 4 (2010) 3580-3589.

13. Kohler, A. R., Som, C., Hellanda, A., and Gottschalk, F., Studying the potential release of carbon nanotubes throughout the application life cycle, J. Cleaner Prod., 16 (2008) 927-937.

14. Nowack, B., et al., Potential scenarios for nanomaterial release and subsequent alteration in the environment, Env. Toxicol. Chem., 31 (2012) 50-59.

15. Nowack, B., Potential release scenarios for carbon nanotubes used in composites. Environment International 59 (2013)1-11.

16. Schlagenhauf, L., et al. Release of carbon nanotubes from an epoxy-based nanocomposite during an abrasion process, *Environ. Sci. Technol.*, 46(13) (2012)7366-7372.

17. Bello, D., et. al., Exposure to nanoscale particles and fibers during machining of hybrid advanced composites containing carbon nanotubes. J. Nanopart. Res., 11 (2009) 231-249.

18. Bello, D., et al., Characterization of exposures to nanoscale particles and fibers during solid core drilling of hybrid carbon nanotube advanced composites. Int. J. Occup. Envir. Health, 16(4) (2010) 434-450.

19. Gohler, D., et al., Characterization of nanoparticle release from surface coatings by the simulation of a sanding process. Ann. Occup. Hyg., 54 (2010) 615-624.

20. Vorbau, M., Hillemann, L. and Stintz, M., Method for the characterization of the abrasion induced nanoparticle release into air from surface coatings, J. Aerosol Sci., 40 (2009) 209-217.

21. Golanski, L., et. al., Characterization of abrasion-induced nanoparticle release from paints into liquids, J. Phys. Conf. Ser. 304 (2011) 012062.

22. Sachse, S., et al., The effect of nanoclay on dust generation during drilling of PA6 nanocomposites, J. Nanomaterials, 2012, DOI10.151155/2012/189386.

23. Kamal, M. and Huang, B., Natural and artificial weathering of polymers. In *Handbook of Polymer Degradation*, Hamid, S., Amin, M.; Maadhah, A., Eds. Marcel Dekker: New York, 1992; pp 127-178.

24. Nguyen, T., et al., Characterization of surface accumulation and release of nanosilica during irradiation of polymer nanocomposites by ultraviolet light, J. Nanosci. & Nanotech., 12 (2012) 6202-6215.

25. Wohlleben, W., et al., A pilot interlab comparison of methods to simulate aging of nanocomposites and to detect fragments released, to be submitted to Env. Sci. Technol.

26. Wohlleben, W., et al., On the life cycle of nanocomposites: comparing released fragments and their in-vitro hazards from three release mechanims and four nanocomposites, Small, 7 (2011) 2384–2395.

27. Petersen, E. J., et al., Methods to assess the impact of UV irradiation on the surface chemistry and structure of multiwall carbon nanotube epoxy nanocomposites, Carbon, 69 (2014) 194-205.

28. Chin, E., et al., Accelerated UV weathering device based on integrating sphere technology, Review Sci. Instr., 75 (2004) 4951.

29. Harrick, N. J*., Internal reflection spectroscopy.,* 2nd ed., Harrick Scientific Corporation, Ossining, NY, 1979, p 30.

30. Rabek, J. F., *Polymer Photodegradation: Mechanism and Experimental Methods*, Chapman & Hall: NY, 1995; pp 185-216.

31. Bellenger, V.; Verdu, J., Oxidative skeleton breaking in epoxy-amine networks, J. Appl. Polym. Sci., *30*(1985)363-374.

32. Rivaton, A., Moreau, L., Gardette, J. L., Photo-oxidation of phenoxy resins at long and short wavelengths - Mechanisms of formation of photoproducts, Polym. Degrad. Stab., *58* (3)(1997) 333-339.

33. Mailhot, N., Morlat-Theias, S., Ouahioune, M., Gardette, J. L., Study of the degradation of an epoxy/amine resin, 1 Photo- and thermo-chemical mechanisms, Macromol. Chem. Phys., 206 (5)(2005) 575-584.

34. Nguyen, T., et al., Degradation modes of crosslinked coatings exposed to photolytic environment, J. Coat. Technol. Res. 10(1) (2013)1-14.

35. Gu, et al., in "Service Life Prediction of Polymeric Materials, Global Perspectives", Eds. J. W. Martin, R. A. Ryntz, J. Chin, R. A. Dickie, Springer, NY., 2009, p. 1.

36. Colthup, N.B., Daly, L.H. and Wiberley, S.E., Introduction to Infrared and Raman Spectroscopy, 3rd ed., Academic Press, N.Y., 1990, p 355.

37. Palmese, G.R. and McCoullough,R.L., Kinetic and thermodynamic considerations regarding interphase formation in thermosetting composite systems., J. Adhesion, 44 (1994) 29-49.